MATERIALS SCIENCE

Bioinspired photocontrollable microstructured transport device

Emre Kizilkan,[1]* Jan Strueben,[2,3,4] Anne Staubitz,[2,3,4]* Stanislav N. Gorb[1]*

Geckos, which can walk upside down on vertical and underneath horizontal surfaces, owe this ability to the hierarchical structures under their toes. These structures are responsible for substantial adhesion and, at the same time, for quick detachment by mechanical stimulus through leg movements. Inspired by such stimuli-responsive systems in nature, we developed an artificial, photocontrollable microstructured transport device. Through tunable ultraviolet light illumination, the adhesive ability of this bioinspired transport device is reduced up to a factor of 2.7 in terms of adhesive forces and is quickly recovered when the light stimulus ceases. This bioinspired photocontrollable device has been used in a pick-up and drop-down system for transporting planar and three-dimensional solid objects.

INTRODUCTION

Highly dynamic attachment and detachment movements are crucial for the legged locomotion of numerous animal species in nature. To allow the locomotion of animals across a surface, two opposing requirements must be achieved: While ensuring substantial adhesion when touching down with the foot, quick detachment is required when the foot needs to move forward. It is well established that, in this process, a hierarchical surface topography plays the main role (*1*–*4*). For example, geckos have fibrillar setae that branch out into spatula-shaped nanostructures. This fibrillar hierarchical structure has a nonsticky default state that can be switched to adhesive state through the action of the shear force using leg movements (*5*). This mechanical stimulus induces fibrillar structures to rearrange themselves and establish an adhesive contact with the substrate. Inspired by such stimuli-responsive adhesive systems in nature, artificial, switchable adhesive micro/nanostructures can be produced. The stimulus enabling surfaces to switch from an adhesive to a nonadhesive state or vice versa can be mechanical (*6*–*8*), magnetic (*9*, *10*), or thermal (*11*–*13*). Besides these, light is a stimulus that can be controlled very quickly and precisely (e.g., in time, intensity, and wavelength), it is a very attractive stimulus for developing bioinspired photoresponsive reversible adhesive systems.

Such a material would need to be prepared from a light-responsive material. One class of materials consists of azobenzene-containing cross-linked liquid crystalline elastomers (LCEs) (*14*). The azobenzene moiety can rapidly alter its molecular dimension, when illuminated with 320- to 380-nm ultraviolet (UV) light, depending on the substituent of the azobenzene. This dimensional change is a consequence of a reversible trans-cis isomerization; the film can then recover its initial shape either by illumination with light wavelengths of 420 to 480 nm (visible light) or by thermal stimuli. As a consequence of the orientational changes of azobenzene-containing liquid crystal phases, macroscopic deformations of the material can be triggered. Therefore, these photoresponsive materials have been used as muscle-like force actuators and light-driven robots (*15*–*17*). Recently, it was shown that porous azobenzene-containing LCEs demonstrate a higher degree of photoinduced macroscopic deformations than pore-free LCEs while retaining similar force actuation properties (*18*).

The utilization of LCEs in bioinspired microstructured dry adhesives is still a challenge for applications. Previous attempts of LCEs for adhesion control used the thermoresponsive features of LCEs (*11*, *12*). These attempts required stimuli high above room temperature at up to 60° to 90°C, which restricts the applicability of the material for technology.

Here, we demonstrate a bioinspired photocontrollable microstructured transport device (BIPMTD). It was designed to use the LCEs as a photocontrolling unit, which would operate at moderate temperatures in combination with a microstructured adhesive top layer made of polydimethylsiloxane (PDMS). Through illumination of UV light, the BIPMTD minimizes its contact area and corresponding adhesive ability. Without the need for a complicated pneumatic/electronic controlling system or any other stimulation, the BIPMTD can recover its initial adhesive state when the UV light illumination ceases. Moreover, the tunable parameters of UV light enable a controllable adhesive ability for BIPMTD. These features provide different utilization possibilities for BIPMTD e.g., pick-and-drop systems for solid objects or robotic designs.

RESULTS

The BIPMTD consisted of three layers: (i) on the surface, mushroom-shaped adhesive microstructures (MSAMSs) protruding from a PDMS layer; (ii) a porous photoresponsive LCE film underneath; and (iii) a PDMS backing layer sealing the LCE film from below (Fig. 1A). The adhesive microstructures and backing layer, made of PDMS, were tightly interconnected to each other through the porous LCE film between them. As an adhesive surface, MSAMS was used, which has been shown previously to have a superior strong but reversible adhesion compared with other bioinspired microstructures made of the same material (*19*–*21*). The MSAMS pillars were 70 μm in height, 45 μm in width at the top, and 35 μm in diameter at the base. Individual MSAMS pillars covered 50% of the apparent surface area (Fig. 1, B and C). Each three layers—the PDMS under MSAMS, LCE film, and sealing PDMS—have a thickness of 100 μm.

An important issue for BIPMTD was to determine whether and to which degree a photostimulus would lead to a geometrical deformation of the BIPMTD, translating into a change in the adhesive force.

[1]Department of Functional Morphology and Biomechanics, Zoological Institute, Kiel University, Am Botanischen Garten 1-9, 24118 Kiel, Germany. [2]Otto Diels Institute for Organic Chemistry, Kiel University, Otto-Hahn-Platz 4, 24118 Kiel, Germany. [3]Institute for Organic and Analytical Chemistry, University of Bremen, Leobener Straße NW 2 C, 28359 Bremen, Germany. [4]MAPEX Center for Materials and Processes, University of Bremen, Bibliothekstraße 1, 28359 Bremen, Germany.
*Corresponding author. Email: ekizilkan@zoologie.uni-kiel.de (E.K.); staubitz@uni-bremen.de (A.S.); sgorb@zoologie.uni-kiel.de (S.N.G.)

For this purpose, force measurement tests with six samples were performed with and without UV light illumination. The outer edges of the BIPMTD samples with dimensions of 10 mm × 1.5 mm × 0.37 mm were fixed onto a glass slide, with the MSAMS pillars pointing upward. However, the middle of the BIPMTD samples was unattached, thereby allowing it to move in a direction perpendicular to the surface. A sapphire glass sphere (Ø = 1 mm) was attached to a force sensor controlled by a micromanipulator. This glass sphere was then brought into contact on top of the MSAMS pillars by applying a preload of 6 mN (see the Supplementary Materials for details). In this way, characteristic force-time data could be acquired for the adhesive contact between the glass sphere and flat BIPMTD sample (Fig. 2A). Normal adhesion (no UV light illumination) was measured by separating the glass sphere from the MSAMS surface by driving the micromanipulator in a perpendicular direction away from the BIPMTD surface with a speed of 200 μm/s. To test the adhesive performance of the BIPMTD sample under a photostimulus, the glass sphere was again brought into contact with the microstructured surface by using the same preload of 6 mN. A narrow-pass UV light source was used to illuminate the BIPMTD samples (Fig. 2B). Subsequently, the glass sphere was separated from the BIPMTD surface under UV light illumination.

The adhesive force measurement (Fig. 2A) showed that the normal adhesion force (no UV) was, on average, 0.73 ± 0.23 mN. When the UV light source was switched on, a light-driven load was observed; the final adhesion under UV light stimulation decreased, on average, to 0.27 ± 0.03 mN (Fig. 2B). When the UV light was turned off again, the expansion of LCE ceased and the BIPMTD displayed a self-shape recovery without any illumination or additional thermal stimulation (see movie S1).

Next, we examined whether controlling the intensity of the light stimulus could be used to adjust the strength of the adhesion. Therefore, the intensity dependence of the geometrical deformation of the BIPMTD was observed by tracing the movement of a reference point in the middle of the sample under different UV light transmission conditions (Fig. 2C and movie S2). Furthermore, the corresponding light-driven forces and adhesive forces were measured (Fig. 2, D and E). These experiments were performed by using band-pass interference filters with 25, 50, and 90% UV light transmissions between the light source and the BIPMTD. The expansions of the film at the reference point were recorded after 30 s of the UV light illumination through the corresponding filters.

After illumination with UV light of controlled intensity, the geometrical deformations in the middle of the BIPMTD sample with respect to a reference point were calculated to be 61.4, 122.9, 150.3, and 181.5 μm for 25, 50, 90, and 100% (no filter) UV light transmissions, respectively. In addition, the engineering strain values were obtained by measuring the lateral length before and after UV light stimulations (see the Supplementary Materials). The engineering strains were 0.0045, 0.019, 0.0252, and 0.031 for 25, 50, 90, and 100% UV light transmissions, respectively. By using these strain values, the angles of the curvature were calculated as 41.99°, 88.58°, 96.06°, and 97.86° for 25, 50, 90, and 100% UV light transmissions, respectively (see fig. S3 for the model and calculations).

To quantify the influence of the light intensity during the deformations, we also measured the corresponding light-driven forces and adhesion forces (Fig. 2, D and E). The light-driven forces were obtained after a preload of 6 mN was applied. These light-driven loads were 6.39 ± 0.07, 7.14 ± 0.09, 8.67 ± 0.06, and 12.14 ± 1.05 mN for 25, 50, 90, and 100% (no filter) UV light transmissions, respectively (Fig. 2D). It was found that a higher transmission of UV light induced a higher preload applied onto the BIPMTD in contact with the glass sphere. The adhesion forces corresponding to these light-driven load measurements were plotted as relative adhesion to normal adhesion (UV off, 1.0). These relative adhesion values were 0.93 ± 0.12, 0.83 ± 0.14, 0.46 ± 0.2, and 0.23 ± 0.02 mN for 25, 50, 90, and 100% (no filter) UV light transmissions, respectively (Fig. 2E). The one-way analysis of variance (ANOVA) Tukey's test results in comparison to normal adhesion values were $P = 0.614$, $P = 0.594$, $P = 0.03$, and $P < 0.01$ for the measurements under 25, 50, 90, and 100% UV light transmissions, respectively.

Another aspect of the light stimulus is that it can be also used to create an adhesive contact. In this experiment, the BIPMTD and the glass sphere (diameter, 1 mm) were placed apart, but at a distance smaller than the one expected for the light-driven deformation (50 μm), where the sphere was fixed and connected to the force sensor (Fig. 3). Then, UV light illumination was applied, which caused the BIPMTD to bend toward the sphere and thus close the gap between itself and the sphere, leading to an adhesive contact. This setup allowed the quantification of the contact bridging and adhesive forces before detachment of two surfaces. When the distance between the BIPMTD and the glass sphere closed, the rest of the expansion reflected as compression force, which corresponds to a preload (F_{pre} = 1.3 mN) for an adhesive contact. When the UV light was turned off, the BIPMTD started to contract again and the glass sphere detached from the MSAMS surface, thereby resulting in an adhesive force peak (F_{adh} = 0.85 mN). Repeatedly turning on/off of the UV light source led to adhesive contact building and detachment without the need for illumination with visible light to induce the cis-trans photoisomerization of azobenzene units in the LCE.

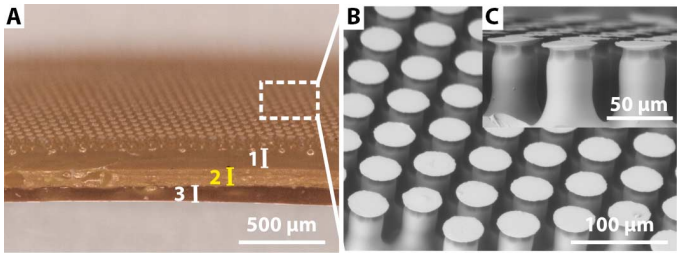

Fig. 1. Microscopy images of the BIPMTD. (**A**) The BIPMTD consists of three layers: (1) a PDMS layer with protruding MSAMS, (2) a porous LCE film, and (3) a PDMS backing layer for the integration of the LCE layer within the BIPMTD. (**B**) Scanning electron microscopy image of the MSAMS pillars at the top of the BIPMTD. (**C**) Lateral view on the individual MSAMS pillars.

DISCUSSION

The three-layered design of the BIPMTD enabled an easy integration of the LCE film inside the PDMS matrix. Interconnecting low surface energy PDMS layers through porous framework minimized possible disjunction problems, because the BIPMTD had to undergo many cycles of shape changes (*22*, *23*). Moreover, this design allowed defect-free ejection of the multilayered composite material from the production template.

The UV light stimulation had several influences on the BIPMTD. As indicated by a previous work (*18*), the LCE film used has a mesogen alignment perpendicular to its surface area. In this ordered mesogenic phase, azobenzene moieties have trans isomeric state in the LCE.

Under UV light illumination, the azobenzene moieties in the trans state photochemically isomerize into the cis state. This photoisomerization disrupts the ordered liquid crystal mesogen alignment, because the cis state demonstrates a nonmesogenic state due to its bend molecular geometry (*14*). Therefore, the LCE experiences a shape change inside the BIPMTD through the photoisomerization of azobenzene. This change of the LCE film induces an elongation along the length inside the BIPMTD, which was fixed from its outer edges on the glass slide. Because of the fixed position of edges of the BIPMTD on the glass slide, the elongation of the LCE generates an expansion of the BIPMTD in perpendicular direction to glass slide surface. This expansion reduces the adhesive contact area between

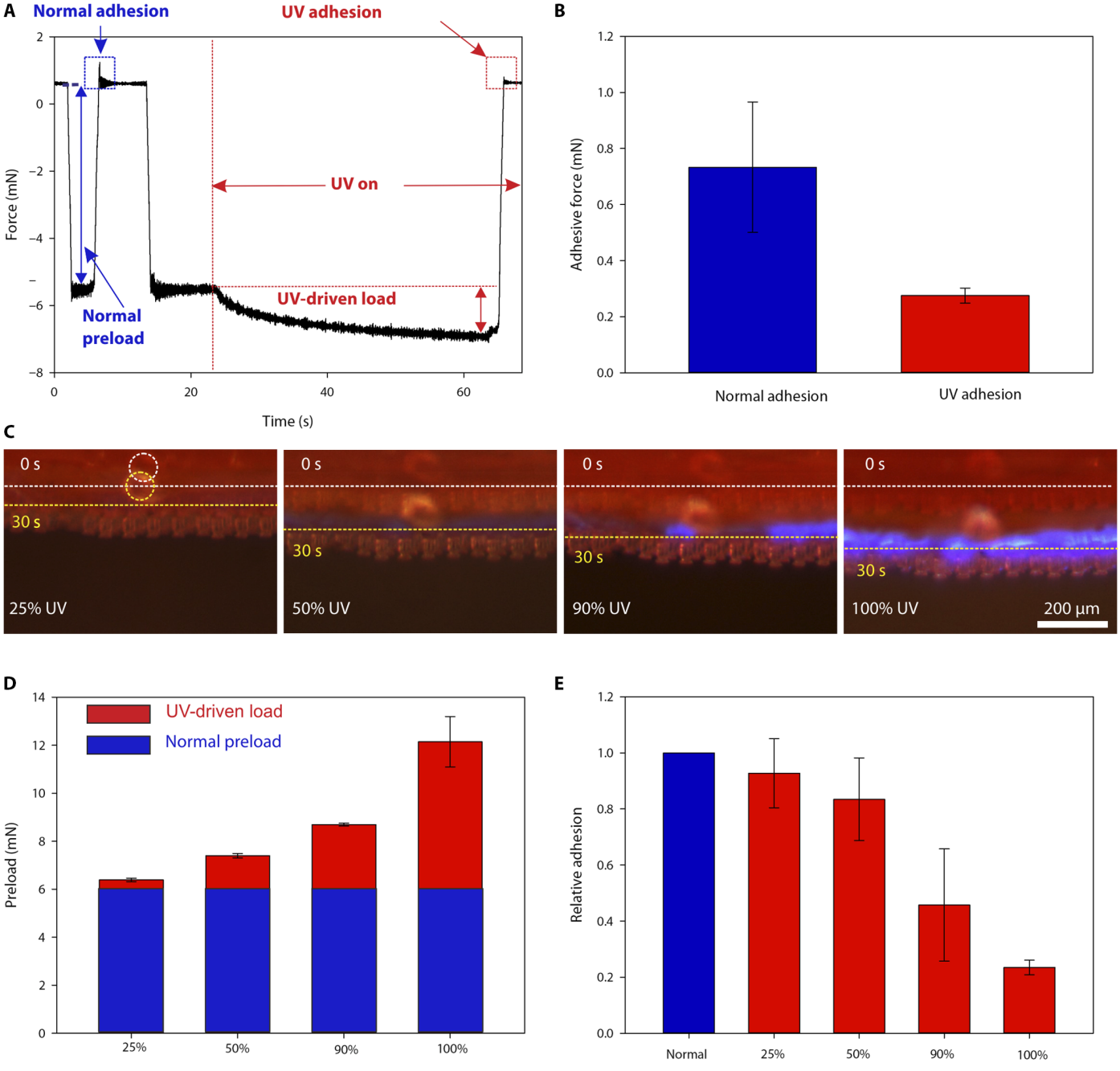

Fig. 2. Mechanical control of the BIPMTD under UV light stimulation. (**A**) Typical adhesive force measurement. A preload was applied to bring the two surfaces into contact. Under UV light illumination, an extra load was obtained (UV-driven). (**B**) Comparison of adhesive forces with and without UV light stimulation. The adhesive force difference between these two cases is statistically significant. (**C**) Influence of light transmission on the BIPMTD was observed by comparing a reference point before (t = 0 s; white point and the dashed line under it) and after 30 s (yellow point and the dashed line under it) under UV light illumination through band-pass interference filters. (**D**) Influence of light transmission on the preload. (**E**) UV light transmission influence on the adhesion of the BIPMTD. The adhesive forces under 25, 50, 90, and 100% (no filter) UV light transmissions are displayed relative to the average of normal adhesion force in (B).

the glass sphere and the BIPMTD: The number of the MSAMS pillars in the area of the firm contact to the glass sphere is minimized. Thus, the expansion generates a compressive force perpendicular to the film in contact to the glass sphere. This force induces MSAMS pillars to be partially squeezed, peeled off, and detached from the round glass surface (Fig. 4).

When the UV light is turned off, the expansion of LCE ceases and the BIPMTD recovers its initial shape without any illumination of visible light. This self-shape recovery of the BIPMTD may arise because of (i) the elastic energy stored during the elongation in the plane and the contraction in thickness of the LCE in the surrounding PDMS and (ii) the absorption of UV light by the azobenzene LCE layer, which initiates the cis-trans isomerization thermally. The high UV absorption ability of azobenzene units in LCE led to an internal temperature increase inside the BIPMTD (fig. S4). The thermally driven cis-trans isomerization is known to be slower than the trans-cis photoisomerization. In the micrometer-sized of the LCE layer, the thermal cis-trans isomerization of azobenzene may occur faster in comparison to macroscale because of the higher inertia of the latter (*24*, *25*). The relative thickness of the LCE layer and the PDMS layers is designed to allow a material to be elastic enough to recover its shape quickly and, at the same time, contribute isomerization of the azobenzene from cis to trans state thermally. Because the PDMS is a good heat insulator (*26*), diffusion of heat is slow, and thus, this surrounding of LCE layers contributes to thermal cis-to-trans isomerization. Therefore, this shape recovery is fast: It starts as soon as the light source is turned off. Despite light-induced internal temperature increase, the external thermal stimuli were minimized by using narrow-pass UV light source and a glass slide between the BIPMTD samples during the measurements and imaging.

By tuning the percentage of UV light transmission, the light-driven load enabled a controllable adhesive contact area and the corresponding adhesive forces. The mechanical measurements show conclusively that a light-driven force induced a higher preload, leading to a lower adhesion of the BIPMTD. Higher light transmissions induced higher forces acting perpendicular on the adhesive contact, disrupted the firm adhesive contact by increasing the number of peeling off, and detached MSAMS pillars from the glass sphere surface. This feature of the BIPMTD means that it not only is an on-off actuator but also can be easily fine-tuned by the applied light intensity. The strain and angle of curvature values indicated that this UV illumination led to lengthening of the material and the corresponding angle of curvature, as the BIPMTD was fixed at its edges. The statistical analysis of adhesion test showed that the critical angle of curvature for significant adhesion change is predicted to start between 88.58° (50% transmission) and 96.06° (90% transmission) of curvature.

To demonstrate the adhesive contact building via photostimulus, we brought the BIPMTD, which was fixed onto the UV light source, to 50-μm distance to a 1-mm glass sphere that was on a PDMS surface (Fig. 5A and movie S3). With the UV light illumination, the BIPMTD came into contact with the sphere. When the UV light illumination stopped, the BIPMTD lifted the sphere up from the PDMS surface. The BIPMTD was driven laterally above an MSAMS structured PDMS surface. Under UV light illumination, the sphere was brought into contact to the MSAMS surface and released when the UV light illumination was turned off.

Thus, the photocontrollable adhesive ability of the BIPMTD should enable it to be used as a pick-and-drop device (Fig. 5B). For this purpose, the BIPMTD was fixed onto a glass slide and attached onto the tip of a UV light source. A circular glass cover slide was engaged with the BIPMTD and has been lifted up (Fig. 5B, i to iv, and movie S4). When the UV light source was turned on, the contact area decreased because of the expansion of the BIPMTD. This led to the partial detachment of the MSAMS from the glass cover slide surface. Furthermore, the BIPMTD could be used to handle much larger three-dimensional (3D) objects. For example, an empty Eppendorf tube could be lifted and dropped via control of the UV light illumination (Fig. 5B, v to viii, and movie S5). Without using any complicated and expensive manipulation setups, the BIPMTD has versatility for transporting planar and 3D solid objects.

To summarize, photocontrollability enables the BIPMTD to either create an adhesive contact or trigger a detachment from the different substrates, depending on the setup. In addition, the BIPMTD does not require stimulation to recover its initial shape because of its muscle-like structure. Previous temperature-responsive LCE-based adhesive systems demonstrated limited applicability because of very high temperature working ranges for real-world applications. However, the

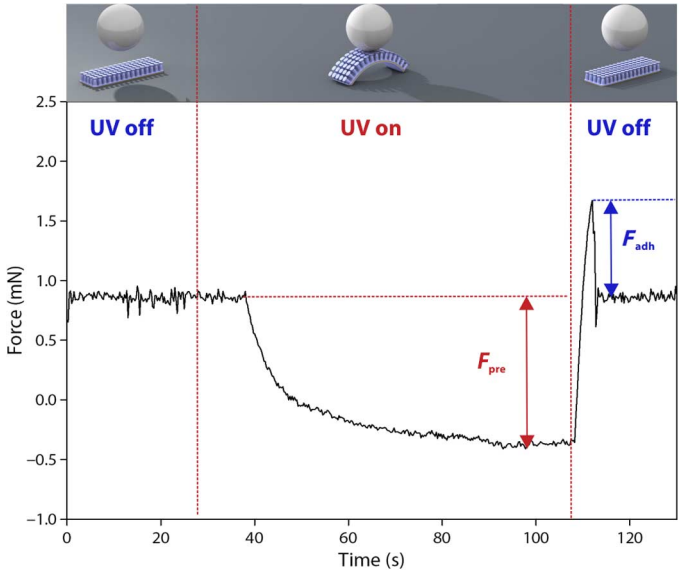

Fig. 3. Force-time diagram during a contact building between the BIPMTD and a fixed glass sphere connected to a force sensor. At a distance of 50 μm, the UV light illumination allowed the BIPMTD to expand and build a contact to a glass sphere (Ø = 1 mm) while demonstrating adhesive preload (F_{pre}). When the UV source was turned off, the BIPMTD started to contract, detach from the glass sphere, and demonstrate an adhesive force peak (F_{adh}).

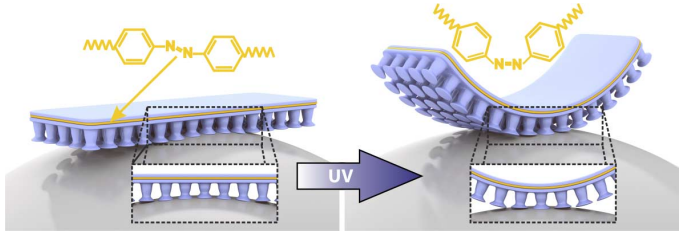

Fig. 4. Influence of the molecular shape change of azobenzene units in the LCE layer to the adhesive contact of the BIPMTD. Because of the shape change of azobenzene units by photoisomerization, the BIPMTD expands onto the glass sphere surface and its contact area decreases with the gradual detachment of adhesive pillars.

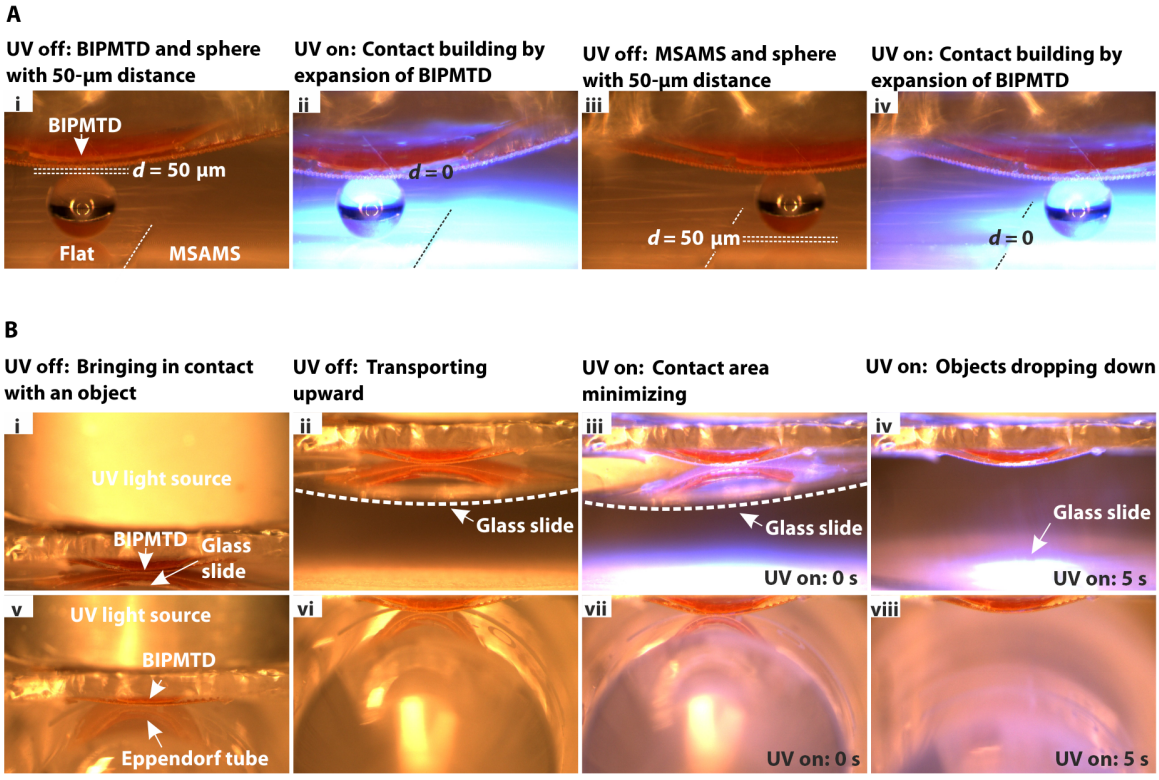

Fig. 5. BIPMTD can be used as a pick-and-drop structure for real-world applications. (**A**) Demonstration of the transportation of a glass sphere (Ø = 1 mm) through contact building caused by UV illumination of the BIPMTD (i to iv) (see also movie S3). On a flat surface, UV light enabled the BIPMTD to expand and come into contact with the glass sphere, which was on a flat PDMS film (i to ii). After lateral transportation of the glass sphere by BIPMTD above the MSAMS structured surface with a micromanipulator, the expansion of the BIPMTD brought the sphere into contact with the structured surface when illuminated by UV light (iii to iv). (**B**) The BIPMTD was used as a pick-and-drop device for a circular glass slide (i to iv) and an Eppendorf tube (v to viii): bringing into contact (i and v), picking up (ii and vi), turning on the UV (iii and vii), and dropping (iv and viii) (see also movies S4 and S5).

BIPMTD provides an easy, residue-free, photoswitchable adhesion, based on the MSAMS surface made of PDMS, which is a versatile material for a vast range of applications. Therefore, we believe that the BIPMTD is suitable for the transportation of planar and nonplanar objects of different sizes for technological areas ranging from robotics to the industrial micromanipulation tools.

MATERIALS AND METHODS

Fabrication

The template for MSAMS pillars was produced using Gecko-Tape (Gottlieb Binder GmbH) and a two-step molding method (*27*): A PDMS prepolymer mixture (10:1 base-curing agent, to produce PDMS layer with an elastic modulus of 1.8 MPa; Sylgard 184, Dow Corning) was poured into the template (*28*). An azobenzene LCE film produced according to a previous work (*18*), with a porosity of 28% and an effective elastic modulus of 180 kPa, was placed on the pillars. The PDMS prepolymer mixture was also applied on top of the LCE film to produce a backing layer. This structure was then cured at 70°C for 2 hours (for more details, see fig. S1 and the Supplementary Materials).

Images

The images were acquired with a digital microscope (VHX-1000, Keyence) and a scanning electron microscope (TM-3000, Hitachi Ltd.). The geometrical deformation calculations of the BIPMTD through light transmissions were performed with the ImageJ 1.47v software (National Institutes of Health). The movies were recorded with an optical stereomicroscope (Leica MZ 12.5, Leica GmbH), a camera (piA1900-32gc, Basler Vision Technologies), and Exilim EX-F1 (Casio Computer Co. Ltd.).

Force measurements

The force measurements were performed using a custom-made system described in the Supplementary Materials and fig. S2. The light sources (λ = 365 nm; LED Pen, Honle UV Technology) were located at the opposite side of the glass sphere and had an intensity of 500 mW cm^{-2}. For the transmission experiment, three different short-pass filters were used, which allowed the transmission of UV light (25% transmission: XB07, Horiba Scientific; 50% transmission: 03FCG001, Melles Griot; 90% transmission: 03SWP402, Melles Griot). The images and the deflection of the BIPMTD under UV light illumination were determined with an optical stereomicroscope (Leica MZ 12.5, Leica GmbH) and a camera (piA1900-32gc, Basler Vision Technologies) connected to it.

Statistical analysis

In Fig. 2 (B, D, and E), the mean values were plotted; the corresponding SDs were displayed by error bars. Eight measurements were performed for each data point. Data obtained from preload and adhesion experiments were statistically analyzed with one-way ANOVA Shapiro-Wilk normality tests using the SigmaPlot 12.5 software (*t* test; SPSS Inc.).

SUPPLEMENTARY MATERIALS

robotics.sciencemag.org/cgi/content/full/2/2/eaak9454/DC1

Movie S1. The volume change of the BIPMTD under UV light illumination.

Movie S2. The observation of the BIPMTD illuminated for 30 s through different UV filters with transmissions of 25, 50, 90, and 100% (no filter).

Movie S3. Transportation of a glass sphere (Ø = 1mm) through UV light–driven volume change of the BIPMTD.

Movie S4. Demonstration of the BIPMTD as a pick-and-drop material for a circular glass slide with a diameter of 15 mm and a thickness of 0.12 mm.

Movie S5. Demonstration of the BIPMTD as a pick-and-drop material for an empty Eppendorf tube (XC63.1, Carl Roth GmbH + Co. KG) with a volume of 1.5 ml.

Fig. S1. Fabrication steps for obtaining the BIPMTD.

Fig. S2. Custom-made setup for adhesion measurement of the BIPMTD under UV light illumination.

Fig. S3. The model for calculation of the angle of curvatures after UV illumination on the BIPMTD.

Fig. S4. Observation of temperature changes of BIPMTD and PDMS samples during UV light illuminations.

Fig. S5. Continuous UV light illumination of the BIPMTD in contact to a force sensor.

REFERENCES AND NOTES

1. M. Kamperman, A. Synytska, Switchable adhesion by chemical functionality and topography. *J. Mater. Chem.* **22**, 19390–19401 (2012).
2. H. Gao, X. Wang, H. Yao, S. Gorb, E. Arzt, Mechanics of hierarchical adhesion structures of geckos. *Mech. Mater.* **37**, 275–285 (2005).
3. G. Huber, H. Mantz, R. Spolenak, K. Mecke, K. Jacobs, S. N. Gorb, E. Arzt, Evidence for capillarity contributions to gecko adhesion from single spatula nanomechanical measurements. *Proc. Natl. Acad. Sci. U.S.A.* **102**, 16293–16296 (2005).
4. G. Huber, S. N. Gorb, R. Spolenak, E. Arzt, Resolving the nanoscale adhesion of individual gecko spatulae by atomic force microscopy. *Biol. Lett.* **1**, 2–4 (2005).
5. K. Autumn, How gecko toes stick: The powerful, fantastic adhesive used by geckos is made of nanoscale hairs that engage tiny forces, inspiring envy among human imitators. *Am. Sci.* **94**, 124–132 (2006).
6. M. Varenberg, S. Gorb, Shearing of fibrillar adhesive microstructure: Friction and shear-related changes in pull-off force. *J. R. Soc. Interface* **4**, 721–725 (2007).
7. K. Dening, L. Heepe, L. Afferrante, G. Carbone, S. N. Gorb, Adhesion control by inflation: Implications from biology to artificial attachment device. *Appl. Phys. A* **116**, 567–573 (2014).
8. S. Song, M. Sitti, Soft grippers using micro-fibrillar adhesives for transfer printing. *Adv. Mater.* **26**, 4901–4906 (2014).
9. D.-M. Drotlef, P. Blümler, A. del Campo, Magnetically actuated patterns for bioinspired reversible adhesion (Dry and Wet). *Adv. Mater.* **26**, 775–779 (2014).
10. A. G. Gillies, J. Kwak, R. S. Fearing, Controllable particle adhesion with a magnetically actuated synthetic gecko adhesive. *Adv. Funct. Mater.* **23**, 3256–3261 (2013).
11. J. Cui, D.-M. Drotlef, I. Larraza, J. P. Fernández-Blázquez, L. F. Boesel, C. Ohm, M. Mezger, R. Zentel, A. del Campo, Bioinspired actuated adhesive patterns of liquid crystalline elastomers. *Adv. Mater.* **24**, 4601–4604 (2012).
12. H. Shahsavan, S. M. Salili, A. Jákli, B. Zhao, Smart muscle-driven self-cleaning of biomimetic microstructures from liquid crystal elastomers. *Adv. Mater.* **27**, 6828–6833 (2015).
13. S. Reddy, E. Arzt, A. del Campo, Bioinspired surfaces with switchable adhesion. *Adv. Mater.* **19**, 3833–3837 (2007).
14. H. Yu, Recent advances in photoresponsive liquid-crystalline polymers containing azobenzene chromophores. *J. Mater. Chem. C* **2**, 3047–3054 (2014).
15. T. J. White, D. J. Broer, Programmable and adaptive mechanics with liquid crystal polymer networks and elastomers. *Nat. Mater.* **14**, 1087–1098 (2015).
16. T. H. Ware, M. E. McConney, J. J. Wie, V. P. Tondiglia, T. J. White, Voxelated liquid crystal elastomers. *Science* **347**, 982–984 (2015).
17. Y. Xia, G. Cedillo-Servin, R. D. Kamien, S. Yang, Guided folding of nematic liquid crystal elastomer sheets into 3D via patterned 1D microchannels. *Adv. Mater.* **28**, 9637–9643 (2016).
18. E. Kizilkan, J. Strueben, X. Jin, C. F. Schaber, R. Adelung, A. Staubitz, S. N. Gorb, Influence of the porosity on the photoresponse of a liquid crystal elastomer. *R. Soc. Open Sci.* **3**, 150700 (2016).
19. S. Gorb, M. Varenberg, A. Peressadko, J. Tuma, Biomimetic mushroom-shaped fibrillar adhesive microstructure. *J. R. Soc. Interface* **4**, 271–275 (2007).
20. L. Heepe, S. N. Gorb, Biologically inspired mushroom-shaped adhesive microstructures. *Annu. Rev. Mater. Res.* **44**, 173–203 (2014).
21. A. del Campo, C. Greiner, E. Arzt, Contact shape controls adhesion of bioinspired fibrillar surfaces. *Langmuir* **23**, 10235–10243 (2007).
22. X. Jin, J. Strueben, L. Heepe, A. Kovalev, Y. K. Mishra, R. Adelung, S. N. Gorb, A. Staubitz, Joining the un-joinable: Adhesion between low surface energy polymers using tetrapodal ZnO linkers. *Adv. Mater.* **24**, 5676–5680 (2012).
23. X. Jin, L. Heepe, J. Strueben, R. Adelung, S. N. Gorb, A. Staubitz, Challenges and solutions for joining polymer materials. *Macromol. Rapid Commun.* **35**, 1551–1570 (2014).
24. X.-G. Liang, Z.-Y. Guo, The scaling effect on the thermal processes at mini/microscale. *Heat Transfer Eng.* **27**, 30–40 (2006).
25. A. Buguin, M.-H. Li, P. Silberzan, B. Ladoux, P. Keller, Micro-actuators: When artificial muscles made of nematic liquid crystal elastomers meet soft lithography. *J. Am. Chem. Soc.* **128**, 1088–1089 (2006).
26. D. Erickson, D. Sinton, D. Li, Joule heating and heat transfer in poly (dimethylsiloxane) microfluidic systems. *Lab Chip* **3**, 141–149 (2003).
27. S. N. Gorb, Visualisation of native surfaces by two-step molding. *Microsc. Today* **15**, 44–46 (2007).
28. J. Zhang, S. Xu, E. Kumacheva, Photogeneration of fluorescent silver nanoclusters in polymer microgels. *Adv. Mater.* **17**, 2336–2340 (2005).

Acknowledgments: We thank R. Adelung and R. Herges for the UV light sources. **Funding:** This work was funded by the Collaborative Research Center 677 "Function by Switching" (project C10). This research has also been supported by the Institutional Strategy of the University of Bremen, funded by the German Excellence Initiative. **Author contributions:** E.K. and S.N.G. designed the BIPMTD. E.K. performed the experiments and produced the BIPMTD. J.S., E.K., and A.S. produced the LCE films and designed Figs. 3 and 4. E.K. wrote the manuscript. A.S. and S.N.G. advised on the writing of the manuscript. All authors contributed to the manuscript. **Competing interests:** The authors declare that they have no competing interests. **Data and materials availability:** All data are in the paper or the Supplementary Materials. Contact E.K. for material requests.

Submitted 18 September 2016
Accepted 15 December 2016
Published 18 January 2017
10.1126/scirobotics.aak9454

Citation: E. Kizilkan, J. Strueben, A. Staubitz, S. N. Gorb, Bioinspired photocontrollable microstructured transport device. *Sci. Robot.* **2**, eaak9454 (2017).

Science Robotics

Bioinspired photocontrollable microstructured transport device

Emre Kizilkan, Jan Strueben, Anne Staubitz, and Stanislav N. Gorb

Sci. Robot. **2** (2), eaak9454. DOI: 10.1126/scirobotics.aak9454